

Contents lists available at ScienceDirect

Physica A

journal homepage: www.elsevier.com/locate/physa



Kinetic Monte Carlo simulations of bi-direction pedestrian flow with different walk speeds



Yi Sun

Department of Mathematics and Interdisciplinary Mathematics Institute, University of South Carolina, Columbia, SC 29208, USA

ARTICLE INFO

Article history: Received 7 May 2019 Received in revised form 9 February 2020 Available online 11 February 2020

Keywords: Bi-direction pedestrian flow Kinetic Monte Carlo Walking speed Cellular automata Lane formation

ABSTRACT

This paper presents a two-dimensional (2D) cellular automaton model for bi-direction pedestrian flows with different walk speeds based on the exclusion principle and Arrhenius microscopic dynamics. This model implements pedestrians' movement rules based on each pedestrian's surrounding conditions and their walking preferences and speeds. Although the decision-making process of pedestrians is more complex and adaptive to dynamic conditions than vehicular flows, our rules can reflect the behaviors of pedestrians at the microscale, such as moving forward, stopping to wait, lane switching, passing others, back stepping, etc. while attaining realistic emergent macroscale activity. We employ an efficient list-based kinetic Monte Carlo (KMC) algorithm to evolve the pedestrian system. The simulation results exhibit transitions between three phases: freely flowing, lane formation, and fully jammed phases as a function of initial density of pedestrians. In the phase of lane formation, we can observe the phenomenon that faster pedestrians exceed the slower ones through a narrow walkway. At different phases the relationships of density-flow and density-velocity are different from each other. The KMC simulations reported here are compared with those from other well-known pedestrian flow models and the corresponding empirical results from real traffic.

© 2020 Elsevier B.V. All rights reserved.

1. Introduction

Recently, considerable research has been done on the study of traffic flows in order to understand the mechanisms leading to traffic jams and improve design of traffic networks for efficient transportation systems [1–12]. On the other hand, pedestrian flows have not been studied as extensively as vehicular traffic due to the fact that the pedestrian movements are more complex, which gives rise to a large variety of collective effects and self-organization phenomena that are not observed in vehicular flows. In particular, the pedestrian dynamics with the condition of different walk speeds has not been fully understood. Therefore, it has become a fundamental task to model pedestrian flows [9,10,13–17].

There are several types of models for describing pedestrian flows: (i) Macroscopic fluid-dynamic and gas-kinetic models that treat the pedestrian flow as a compressible fluid formed by the pedestrians and use partial differential equations (PDEs, typically conservation laws) to relate the density and flux of pedestrians [18–24]. (ii) Microscopic noninteger *off-lattice* models that treat pedestrians as particles subject to interactions induced by the social behavior of the individuals. This leads to coupled equations of motion with interactions depending on the distances between them; some important examples include the *social-force* (SF) model [25–27] and the *optimal velocity* (OV) model [28,29]. (iii) Microscopic *cellular automata* (CA) [30,31] models where a lattice site configuration with values 1 (pedestrian is present) and 0 (pedestrian is absent) combined with explicit rules for pedestrian movement on lattice sites is used to represent pedestrian flow.

E-mail address: yisun@math.sc.edu.

Compared with the off-lattice models, CA models are simpler to implement and are more amenable to numerical investigation. Therefore, they have been widely used to represent traffic flow, in particular, vehicular traffic [6,32–38]. Recently, a look-ahead rule was used to model the effect of long-range traffic conditions in a CA model, which was then coarse-grained to derive a macroscopic PDE description with nonlocal interactions [39]. Extensions to multilane and multiclass traffic have also been developed [40,41]. An improved coarse-grained model at the ODE level has been discussed in [42]. Two different look-ahead rules in both one-dimensional (1D) and two-dimensional (2D) CA models were compared in [43,44].

On the other hand, CA models with empirical rules have also been used to simulate the pedestrian dynamics. Blue and Adler [45–48] have extended two-lane variants of the Nagel–Schreckenberg model [33] for the description of pedestrian flows. Fukui and Ishibashi (FI) [49,50] have proposed a model to study bi-directional pedestrian flows in a long corridor. Nagatani and collaborators [51–54] have used variations of the FI model to investigate situations where a jamming transition can occur. In [55,56], the so-called *floor field* model was introduced by Schadschneider and collaborators, which has become a standard CA approach to pedestrian dynamics. In [57,58], Yue et al. have combined the idea of the FI model with that of the floor field model to propose the *dynamic parameter* model, which can obtain more realistic fundamental diagrams. In [59–62], the *pre-fixed probabilities* model was proposed by Fan and collaborators for simulating bi-direction pedestrian movements. Recently Sun [63,64] has employed an efficient list-based kinetic Monte Carlo method to study pedestrian flow models with a same walk speed on 2D lattices.

In this paper, we propose a CA model on 2D lattices to study bi-direction pedestrian flows with different walk speeds. The pedestrians' movement is described using stochastic rules based on the exclusion principle and Arrhenius microscopic dynamics according to the configuration of the surrounding conditions of each pedestrian. Our rules can reflect the pedestrians' decisions of action such as moving forward, stopping to wait, lane switching, back stepping, and the walking preference and speeds. The approach in our model and most of CA models for traffic/pedestrian flows are similar to what has been done in the Ising model for equilibrium systems, and can be viewed as the extension of the Ising model to the non-equilibrium traffic/pedestrian dynamics. The CA models are usually simple and only the basic interactions rules are followed while the Ising model is a model of classical spins and has played an enormous role for statistical physics/mechanics, especially the understanding of phase transitions.

Numerically we employ the kinetic Monte Carlo (KMC) algorithm [65] to simulate the microscopic dynamics of the pedestrian flow for improving computational efficiency due to the main feature of KMC—"rejection-free". When the pedestrian dynamics features a finite number of distinct processes in configurational changes, we develop an efficient list-based KMC algorithm using fast search that can further improve computational efficiency compared to the general KMC method. With reasonable values of the model parameters (the characteristic time unit and the interaction strength), the KMC simulations are used to predict the time evolution of bi-direction pedestrian flows with different walk speeds. The simulation results exhibit transitions between three phases: freely flowing, lane formation, and fully jammed phases as a function of initial density of pedestrians. In the phase of lane formation, we can observe the phenomenon that faster pedestrians exceed the slower ones through a narrow walkway. At different phases, the relationships of density–flow and density–velocity are different from each other. The KMC simulations reported here are compared with those from other well-known pedestrian flow models and the corresponding empirical results from real traffic.

The rest of the paper is organized as follows. In Section 2, we introduce the CA model with pedestrians' interaction rules. In Section 3, the list-based KMC algorithm and its implementation is presented. In Section 4, we provide a series of numerical simulations in various parameter regimes for bi-direction pedestrian flows. We state our conclusions in Section 5.

2. A cellular automaton model

We describe the construction of the cellular automaton model for bi-direction pedestrian flows in a 2D system, which usually takes rectangular domains to represent walking infrastructures such as bridges, channels of subways, corridors in buildings, etc. Here for simplicity, the model is defined on a square lattice with $M \times M$ cells, where M is the system size. The configuration at each cell (x, y) for $1 \le x, y \le M$ is defined by an index $\sigma_{(x, y)}$:

$$\sigma_{(x,y)} = \begin{cases} 0 & \text{if the cell } (x,y) \text{ is empty,} \\ 1 & \text{if a fast eastbound pedestrian occupies cell } (x,y), \\ 2 & \text{if a slow eastbound pedestrian occupies cell } (x,y), \\ 3 & \text{if a fast westbound pedestrian occupies cell } (x,y), \\ 4 & \text{if a slow westbound pedestrian occupies cell } (x,y), \end{cases}$$

$$(1)$$

and the state of the system is represented by the configuration space $\{0, 1, 2, 3, 4\}^{M^2}$. Transitions in the state of this system represent the pedestrian movements, which obey the rules of an exclusion process [66]: two nearest-neighbor lattice cells exchange values in each transition and pedestrians cannot occupy the same cell. In addition pedestrians are allowed to move into only one of the nearest-neighbor cells in one transition. Here, we consider the Moore neighborhood

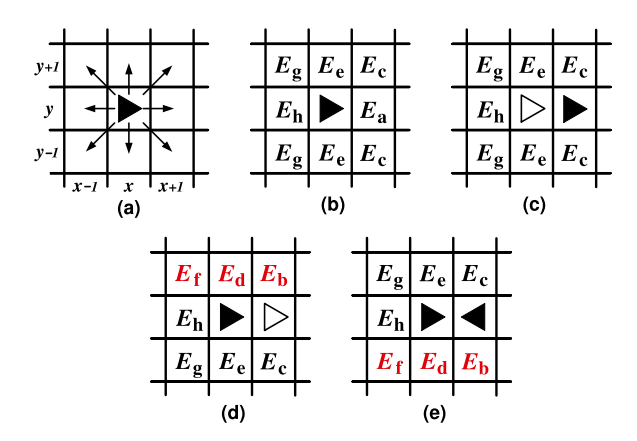


Fig. 1. Schematic representation of pedestrian dynamic rules and parameters. (a): The movement field of an eastbound pedestrian, who may stay at the core cell or move into one of the eight nearest neighboring cells in the Moore neighborhood. (b)–(e): The interaction strength parameters for the pedestrian to move into the corresponding cells in different situations.

which consists eight nearest-neighbor cells [30,31]. For example, the case for a fast eastbound pedestrian at cell (x, y) moving east is of the form (see Fig. 1(a))

$$\{\sigma_{(x,y)} = 1, \sigma_{(x+1,y)} = 0\} \rightarrow \{\sigma_{(x,y)} = 0, \sigma_{(x+1,y)} = 1\}.$$

The transition rate depends on spatial Arrhenius-type interactions with a one-sided interaction and traffic situation around the moving pedestrian. Similarly to the spin-exchange Arrhenius dynamics in which the simulation is driven based on the energy barrier a particle has to overcome in changing from one state to another [39], we perform a pedestrian move as a nearest-neighbor hopping process with its rate given by the Arrhenius relation:

$$r = \omega_0 \exp\left(-E\right),\tag{2}$$

where the prefactor $\omega_0 = 1/\tau_0$ corresponds to the pedestrian moving frequency or speed and τ_0 is the characteristic time. The values of ω_0 and τ_0 take $\omega_{\rm fast}$ and $\tau_{\rm fast}$ for fast pedestrians, or $\omega_{\rm slow}$ and $\tau_{\rm slow}$ for slow pedestrians, respectively. The moving energy barrier E is assumed to depend only on the local environment of the pedestrian under consideration (Fig. 1). In particular, the energy barrier is given by $E = E_{\rm site} + E_{\rm p}$, where $E_{\rm site}$ is the interaction strength associated with the site binding of the pedestrian, which could vary in both space and time to account for spatial and temporal traffic situations (in this study we set $E_{\rm site} = 0$). The parameter $E_{\rm p}$ is the pedestrian interaction strength, which depends on the pedestrian's speed, destination, and his/her moving direction. Based on the formula (2), we can see that the smaller is the energy barrier $E_{\rm p}$, the larger is the transition rate r.

Here we take an eastbound pedestrian (" \blacktriangleright " with the fast speed or " \triangleright " with the slow speed) at the cell (x,y) as an example to illustrate the dynamic rules and parameters. As shown in Fig. 1(b), when the eastbound pedestrian (\blacktriangleright) moves straightforwardly from (x,y) to the east neighboring cell (x+1,y) which is unoccupied, we take $E_p = E_a$; if the eastbound pedestrian moves in the southeast or northeast direction to (x+1,y-1) or (x+1,y+1), we take $E_p = E_c$. Since the destination of the eastbound pedestrians is the east boundary of the square lattice, the pedestrian prefers to choose the cells in the direction towards the east boundary in order to arrive there with a route as short as possible. Therefore, we should make $E_a < E_c$ so that the rate $r_a > r_c$, i.e., the probability of moving straightforward is larger than that of moving into east-diagonal cells. If the eastbound pedestrian chooses to move into his/her left or right cell at (x,y+1) or (x,y-1) in the middle column, he/she will not be able to get any closer to the destination. For this case, we take $E_p = E_e$, which is larger than E_c so that the rate $e_c < e_c$. Similarly, if the eastbound pedestrian chooses to move in the southwest/northwest directions to $e_c < e_c < e_c$. Similarly, if the eastbound pedestrian chooses to move in the southwest/northwest directions to $e_c < e_c < e_c < e_c$. Similarly, if the eastbound pedestrian chooses to move in the southwest/northwest directions to $e_c < e_c < e$

In Fig. 1(c), if a slow eastbound pedestrian (\triangleright) encounters a fast eastbound pedestrian (\blacktriangleright) in the cell at (x+1,y), we take the same moving rules as shown in Fig. 1(b) for the slow eastbound pedestrian except the rule for the direction to move straightforwardly. These rules also hold for the situations when an eastbound pedestrian encounters another eastbound one with the same speed, i.e., the cases of (\triangleright) and (\blacktriangleright).

However, if a fast eastbound pedestrian (\triangleright) encounters a slow eastbound pedestrian (\triangleright) as shown in Fig. 1(d), we need to consider the custom in the countries where pedestrians prefer to exceed slower ones from the left-hand side. For this rule we introduce another three parameters E_b , E_d , and E_f for the moving directions in the northeast, north, and northwest, respectively. Since the pedestrian moves preferably to the left-hand direction in this configuration, we should take $E_b < E_c$ so that the rate $r_b > r_c$, which reflects the attractiveness of the left-hand side positions to the pedestrian

over the right-hand side ones (in other words, reflects the repulsive force from right-hand side positions). Similarly, we take $E_d < E_e$ and $E_f < E_g$ so that the rates $r_d > r_e$ and $r_f > r_g$.

Moreover, in our model we also consider another custom for pedestrians in these countries to walk on the right-hand side of the walkway. Thus we add another rule as shown in Fig. 1(e). If an eastbound pedestrian (▶ or ▷) encounters a westbound pedestrian (◄ or ▷), we use the above parameters E_b , E_d , and E_f for the moving directions in the southeast, south, and southwest, respectively. In this situation we also take $E_b < E_c$, $E_d < E_e$ and $E_f < E_g$ so that the rates $r_b > r_c$, $r_d > r_e$ and $r_f > r_g$, which reflects the attractiveness of the right-hand side positions to the pedestrian over the left-hand side ones (in other words, reflects the repulsive force from left-hand side positions). In other countries where the pedestrians prefer to walk on the left-hand side of the walkway and exceed slower ones from the right-hand side, the contrary rules can be adopted accordingly.

Once we set the values of all eight interaction parameters E_a , E_b , E_c , E_d , E_e , E_f , E_g , E_h , and the two characteristic time parameters τ_{fast} and τ_{slow} ; then all pedestrians' moving events can be classified into 17 (= 2 × 8 + 1) folds according to the corresponding values of the rate r for two types of pedestrians (fast or slow) moving into different neighboring cells or the case of staying at the core cell, as shown in Figs. 1(b)–(e).

In the bi-direction pedestrian flow model, we consider two species of pedestrians moving in opposite directions: the eastbound (\blacktriangleright or \triangleright) and westbound (\blacktriangleleft or \triangleleft). The periodic boundary conditions are applied at the east and west boundaries. For example, if an eastbound pedestrian moves out of the east boundary, he/she will reenter the lattice domain from the west boundary. Both eastbound and westbound pedestrians are inhibited from crossing the north and south boundaries, where closed boundary conditions are adopted. Therefore, the total number of pedestrians in the system is conserved during simulations. In this paper, for each species of pedestrians, we consider the cases with equal numbers of fast and slow pedestrians, i.e., $N_{\blacktriangleright} = N_{\triangleright}$ and $N_{\blacktriangleleft} = N_{\triangleleft}$. Suppose that $N_E = N_{\blacktriangleright} + N_{\triangleright}$ is the total number of the eastbound pedestrians in the system, the density of the eastbound pedestrians is given by $\rho_E = N_E/M^2$. Similarly, $N_W = N_{\blacktriangleleft} + N_{\triangleleft}$ is the total number of the westbound pedestrians and $\rho_W = N_W/M^2$ is the corresponding density. In the simulations, one aspect will be focused on different directional splits of the pedestrians, i.e., different densities of the eastbound ρ_E and westbound ρ_W , with the total density of the pedestrians $\rho_E = \rho_E + \rho_W$.

To summarize, the following parameters need to be given for the stochastic simulations with the pedestrian dynamic rules: (i) the characteristic time parameters τ_{fast} and τ_{slow} ; (ii) the eight strength parameters of pedestrian interactions, E_{a} to E_{h} .

3. The kinetic Monte Carlo method

We apply the kinetic Monte Carlo (KMC) method to the above cellular automaton model to investigate the evolution of the pedestrian system. We choose the KMC instead of the Metropolis Monte Carlo (MMC) method [67] since in the MMC method, trial steps are sometimes rejected because the acceptance probability is small, in particular when a system approaches the equilibrium, or the density of pedestrians is high. The KMC method that we adopt here is related to the method proposed by Bortz, Kalos, and Lebowitz as a speedup to the MMC method for simulating the evolution of Ising models [65]. A main feature of the KMC algorithm is that it is "rejection-free". In each step, the transition rates for all possible changes from the current configuration are calculated and then a new configuration is chosen with a probability proportional to the rate of the corresponding transition. Since the interaction is short ranged within the nearest-neighbors, there is only a small number of local environments that need to be changed due to the previous transition. As the MMC is mainly a way of simulating an equilibrium distribution for a model, the KMC method is more suitable for simulating the non-equilibrium evolution of the pedestrian systems.

The KMC algorithm is built on the assumption that the model features N independent Poisson processes (corresponding to N moving events on the lattice) with transition rates r_i in (2) that sum up to give the total rate $R = \sum_{i=1}^N r_i$. In simulations with a finite number of distinct processes it is more efficient to consider the groups of events according to their rates [68–70]. This can be done by forming lists of the same kinds of events according to the values of E_p and E_p and two different values of E_p and two different values of E_p and two different values of E_p and two two types of pedestrians to move into different neighboring cells and one case of staying at the core cell. Therefore, we can put the total E_p vents into E_p lists (E_p 17), labeled by E_p 17. All processes in the E_p 18 list have the same rate E_p 18 list by E_p 19 lists by E_p 19 lists by E_p 19 lists by E_p 20 lists by E_p 21 lists by E_p 22 lists by E_p 31 lists by E_p 32 lists by E_p 33 lists by E_p 34 lists by E_p 35 lists by E_p 36 lists by E_p 36 lists by E_p 37 lists by E_p 37 lists by E_p 37 lists by E_p 38 lists by E_p 39 lists by E_p 39 lists by E_p 30 lists by E_p 30 lists by E_p 31 lists by E_p 31 lists by E_p 31 lists by E_p 32 lists by E_p 32 lists by E_p 37 lists by E_p 39 lists by E_p 31 lists by E_p 32 lists by E_p 32 lists by E_p 32 lists by E_p 32 lists by E_p 33 lists by E_p 34 lists by E_p 35 lists by E_p 35 lists by E_p 36 lists by E_p 36 lists by E_p 37 lists by E_p 37 lists by E_p 37 lists by E_p 38 lists by E_p 39 lists by E_p 39 lists by E_p 31 lists by E_p 31 lists by E_p 31 lists by E_p 32 lists by E_p 31 lists by E_p 32 lists by E_p 32 lists by E_p 37 lists by E_p 38 lists by E_p 39 lists by E_p 39 lists by E_p 30 lists by E_p 30 list

List-based KMC algorithm.

Step 1: Generate a uniform random number $\xi_1 \in (0, 1)$ and decide which process will take place by choosing the list index s such that

$$\sum_{l=1}^{s-1} \frac{R_l}{R} < \xi_1 \le \sum_{l=1}^{s} \frac{R_l}{R} \tag{3}$$

Step 2: Select a realization of the process s. This can be done with the help of a list of coordinates for each kind of event, and an integer random number ξ_2 in the range $[1, n_s]$; ξ_2 is generated and the corresponding member from the list is selected.

Step 3: Perform the selected event leading to a new configuration.

Step 4: Use R and another random number $\xi_3 \in (0, 1)$ to decide the time it takes for that event to occur (the transition time), i.e., the nonuniform time step $\Delta t = -\log(\xi_3)/R$.

Step 5: Update the multiplicity n_l , relative rates R_l , total rate R and any data structure that may have changed due to that event.

4. Numerical experiments

We next investigate bi-direction pedestrian flows with different walk speeds in various parameter regimes with the numerical method developed in the previous section. Following [10,63,71], we set the physical size of each cell to $0.4 \times 0.4 \,\mathrm{m}^2$, which allows one to keep a minimal distance to others in order to avoid bumping into them. This is consistent to the fact that maximal densities of about 6 peds/m² can be observed in dense crowds [10]. For a fast pedestrian who has an average speed of $v_{\mathrm{fast}} \approx 1.6 \,\mathrm{m/s}$, an estimate of time to cross a cell is given by

$$\Delta t_{\text{fast}} = \frac{0.4 \text{ m}}{1.6 \text{ m/s}} = \frac{1}{4} \text{ s.} \tag{4}$$

In a free-flow regime, we expect all fast pedestrians to move at their desired speed that is set to 4 cells per second ($\approx 1.6 \text{ m/s}$). This is accomplished by setting the characteristic time $\tau_{\text{fast}} = 1/4 \text{ s}$, and then the moving frequency $\omega_{\text{fast}} = 4 \text{ s}^{-1}$. Similarly, we take the average speed of a slow pedestrian $v_{\text{slow}} \approx 1.2 \text{ m/s}$, which corresponds to $\tau_{\text{slow}} = 1/3 \text{ s}$ and $\omega_{\text{slow}} = 3 \text{ s}^{-1}$. In fact, due to the inherent stochasticity in the simulations, sometimes pedestrians may move faster or slower than his/her average speed.

As there are eight interaction strength parameters E_a to E_h to be explored, for simplicity, we take a fixed relationships between them, which is similar to the choice of piecewise constants for short-range local interactions in the look-ahead rules of modeling traffic flow [39,43]. We take $E_a = 0$ and therefore the rate $r = \omega_0 \exp(0) = \omega_0$, thus with the maximum probability of moving straightforward towards the pedestrian's destination. For the other interaction parameters, we simply take $E_b = 2.0$, $E_c = 2.0 + \delta E$, $E_d = 4.0$, $E_e = 4.0 + \delta E$, $E_f = 6.0$, $E_g = 6.0 + \delta E$, and $E_h = 8.0 + \delta E$, where δE corresponds to the strength of repulsion from one-side positions (which is equivalent to the strength of the walking preference for the other side) and its range is $\delta E \in [0, 8.0]$. In all simulations shown in the following Sections 4.1 and 4.2, we set the lattice size to be M = 50. We note that the configurations using other values of the lattice size M produce similar results, which are not shown for the brevity of the presentation. The effect of the system size on the pedestrian flow model and the phase transition has been studied in our previous work [63].

4.1. Numerical comparisons for different strengths of pedestrians' walking preference

First, we perform a series of simulations to analyze the effects of the pedestrians' preference for walking on the right-hand side and exceeding slower ones from the left-hand side. In this section, we take a fixed directional split between the westbound and eastbound pedestrians: $N_W/N_E = 50/50$ (balanced flow), which means that the proportions of the two species of pedestrians in the total pedestrians are same to 50%. At the beginning of each simulation, the pedestrians are randomly distributed on the lattice. The results exhibit a phase transition from the free-flow regime to the completely jammed regime as the total density of the pedestrians ρ increases.

Fig. 2 shows six typical configurations of the bi-direction pedestrian flow with different values of the total density ρ and the strength δE of the walking preference in the range [0, 8.0]. Fig. 2(a) displays a configuration below the transition, i.e., the free-flow phase with a low pedestrian density $\rho=0.1$ and the strength $\delta E=0$, where all four types of the pedestrians (two species and two speeds) are distributed randomly and homogeneously. Fig. 2(b) shows a separated-flow phase with the same density $\rho=0.1$ and an increased strength $\delta E=1.0$. In this situation, the system is self-organized due to the preference for walking on the right-hand side (or the repulsion from the left-hand side positions). There are two regions formed on the lattice: the upper region dominated by the westbound pedestrians and the lower region dominated by the eastbound pedestrians. In each region the fast and slow pedestrians are still mixed and distributed randomly and homogeneously. We note that sometimes there are spontaneously forming jams that are localized in both time and space, particularly between two regions. For example, they may appear in the case with $\rho=0.13$ and $\delta E=1.0$ (configurations not shown for the brevity).

In Fig. 2(c) where the density rises to $\rho=0.25$ at the same strength $\delta E=1.0$, the system is transformed into a completely jammed phase. Here the jammed pedestrians get crowded face to face with the empty areas behind them and there is no channel formed for pedestrians to pass. The boundary between the two types of pedestrians in the jam is irregular. The intrinsic stochasticity of the dynamics triggers the onset of jamming and the phenomenon of complete jamming through self-organization. We remark that different initial distributions of pedestrians may result in different final jammed configurations, where sometimes the eastbound pedestrians may accumulate in the upper region and the westbound pedestrians in the lower region. We have run the simulation shown in Fig. 2(c) till the final time of 2 h, which is long enough to make sure that the jammed phase is not transient.

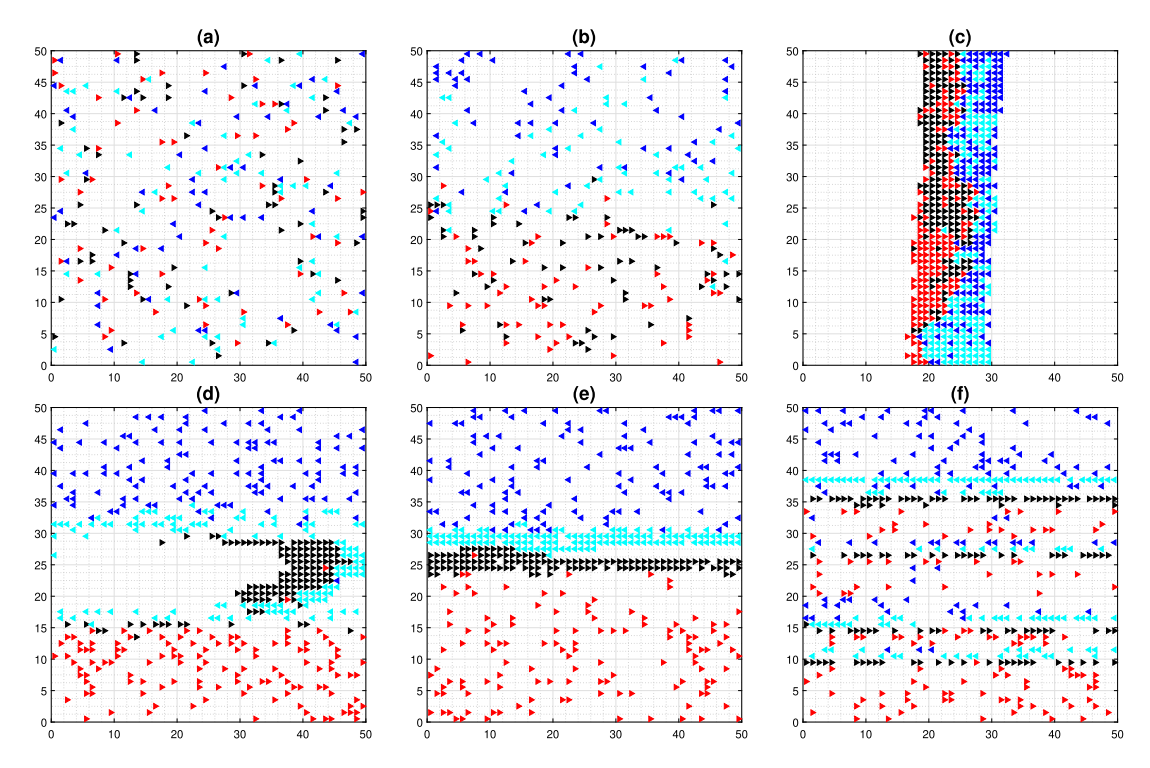


Fig. 2. Typical configurations of the bi-direction fast and slow pedestrian flow on an $M \times M$ lattice of size M=50. The pedestrians are represented by red (\blacktriangleright) for the slow eastbound, black (\blacktriangleright) for the fast eastbound, blue (\blacktriangleleft) for the slow westbound, and cyan (\blacktriangleleft) for the fast westbound, respectively. In all KMC simulations, we take the directional split $N_W/N_E=50/50$, the interaction strengths $E_a=0$, $E_b=2.0$, $E_c=2.0+\delta E$, $E_d=4.0$, $E_c=4.0$, $E_c=4$

As shown in Fig. 2(d) for the density $\rho=0.2$, when the strength reaches $\delta E=3.0$, the system is self-organized into a partially jammed phase with three regions. In the middle region, part of the fast eastbound and fast westbound pedestrians encounter and produce a jam, which blocks part of the walkway. In the upper and lower regions, the slow westbound and slow eastbound pedestrians are homogeneously distributed, respectively. If we keep the same density $\rho=0.2$ and increase the strength to $\delta E=6.0$ in Fig. 2(e), the system enters a lane formation phase, which consists of four zones for the slow and fast westbound pedestrians, and the fast and slow eastbound ones from upper to lower regions on the lattice, respectively. This is not only due to the initial distribution of pedestrians but also due to the pedestrians interactions. Pedestrians moving in a mixed crowd will have frequent interactions with other pedestrians walking in the opposite direction. Even for the pedestrians walking in the same direction, they may move with different speeds and have interactions to each other. Due to the interactions, the encountering pedestrians move a little aside to their right-hand positions by following the traffic rule or custom in order to pass each other. The fast pedestrians also move aside to their left-hand positions to exceed the slow ones walking in the same direction. These sidewards movements tend to separate pedestrians moving in opposite directions and/or with different walking speeds, which forms the lanes.

After we increase the strength further up to $\delta E=8.0$ in Fig. 2(f), the system is self-organized into another lane formation phase with multiple groups of lanes, where each group is composed of four lanes of pedestrians with opposite moving directions and different speeds in the same order from upper to lower as shown in Fig. 2(e) (i.e., the slow and fast westbound, and the fast and slow eastbound). We remark that the simulation of Fig. 2(e) undergoes a time-dependent phenomenon (results not shown for the brevity): at the beginning there were also multiple groups of lanes formatted, later the lanes merged into wider ones (especially for the slow pedestrians) and eventually four separated zones formed. Since in this case we take $\delta E=6.0$ and the repulsion from the side positions are not sufficiently strong, it is still possible for the pedestrians to move sidewards. Thus the 'friction' between zones with opposite moving directions and different speeds could be rather frequent and strong, and the pedestrians prefer to merge into wider lanes in order to reduce the disturbances. On the other hand, in Fig. 2(f) we have $\delta E=8.0$ and the repulsion from the side positions are extremely strong. Therefore, when the same species of pedestrians with the same speed move in one lane, it is very unlikely for them to move sidewards and walk out of the lane. So the tendency to break up existing lanes is negligible and the lanes are very stable [25]. We also note that different initial distributions of pedestrians may result in different number of lanes even they have the same total density.

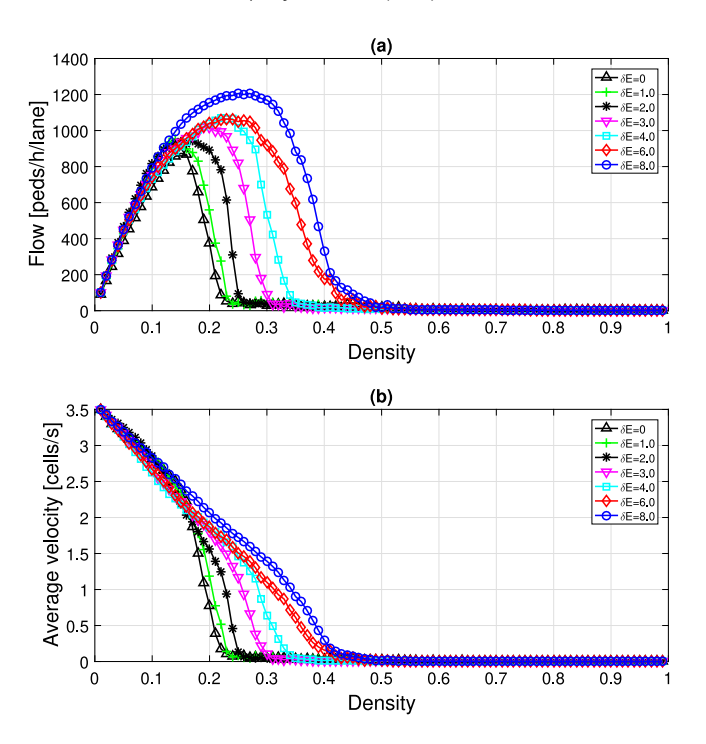


Fig. 3. Comparison results of the bi-direction pedestrian flow model with seven different values of the strength δE of the walking preference from 0 to 8.0. In all KMC simulations, we take the lattice size M=50, the directional split $N_W/N_E=50/50$, the interaction strengths $E_a=0$, $E_b=2.0$, $E_c=2.0+\delta E$, $E_d=4.0$, $E_c=4.0+\delta E$, $E_f=6.0$, $E_g=6.0+\delta E$, $E_h=8.0+\delta E$ and the final time is 2 h. For every value of ρ and δE , we report results averaged over ten simulations with different random number seeds. (a): Long-time averages of the density-flow relationship of pedestrians. (b): Ensemble-averaged velocity of pedestrians versus the density.

In Figs. 2(e) and (f), we also find that the lanes of fast pedestrians are narrower than those of slow pedestrians, which can be observed in experiments of pedestrian flows [10,13,15]. The reason is that the fast pedestrians have more chances for update in the KMC simulations than the slow ones. When the fast pedestrians encounter the slow ones, they may move aside, and the slow ones have more probability to stay and wait. Therefore, the walkway of fast pedestrians is narrower than that of slow pedestrians.

Similar to vehicular traffic, the main characteristic quantities for the description of pedestrian streams are flow and density. To identify the parameter range of the phase transition, we make a series of KMC simulations with different pedestrian densities ranging from $\rho=0.01$ to $\rho=0.99$ until the same final time (2 h). Fig. 3 shows the fundamental diagrams of the density–flow and density–velocity relationships, and compare the results for seven different values of the strength δE of the walking preference from 0 to 8.0 in E_c , E_e , E_g , E_h , while fixing the other interaction strengths $E_a=0$, $E_b=2.0$, $E_d=4.0$, and $E_f=6.0$. For each simulation we compute long-time averages of the flow $\langle F \rangle$ in number of pedestrians crossing a fixed location of a facility per hour per lane and obtain the ensemble-averaged velocity $\langle v \rangle$ in cells per second by averaging the velocities over all pedestrians. The average flow $\langle F \rangle$ of pedestrians is measured as the sum of the eastbound pedestrians passing through the east boundary and the westbound pedestrians passing through the east boundary and the west boundary and

Fig. 3(a) shows that all curves exhibit phase transitions between the free-flow phase and the jammed phase. In the free-flow regime, the value of $\langle F \rangle$ increases as the pedestrian density ρ increases, and reaches its maximum at the critical value, $\rho_{\rm crit}$. Beyond that point, the phase transition starts and the flow drops down to zero as all pedestrians are stopped. Here, certain characteristics are shared by most fundamental diagrams that have been obtained empirically, e.g., a linear increase of the flow at low densities, a single maximum of the flow, and an asymmetry toward smaller densities. These features are similar to the characteristics of fundamental diagrams of vehicular traffic [10,13]. On the other hand, Fig. 3(b) shows that in the free-flow regime the ensemble-averaged velocity $\langle v \rangle$ decreases approximately linearly from the maximum speed of 3.5 cells per second (i.e., ≈ 1.4 m/s) as ρ increases. When ρ is larger than the critical point $\rho_{\rm crit}$, the average velocity also drops down quickly to zero and the density-velocity curve is negative exponential. This linear relationship follows the Greenshields model [72] and the negative exponential relationship belongs to the Underwood model [73].

As the strength δE changes from 0 to 8.0, the transition period during which the flow $\langle F \rangle$ drops down from its maximum to zero shifts to the right (i.e., the value of the critical density $\rho_{\rm crit}$ increases). Meanwhile, the maximum value of the flow

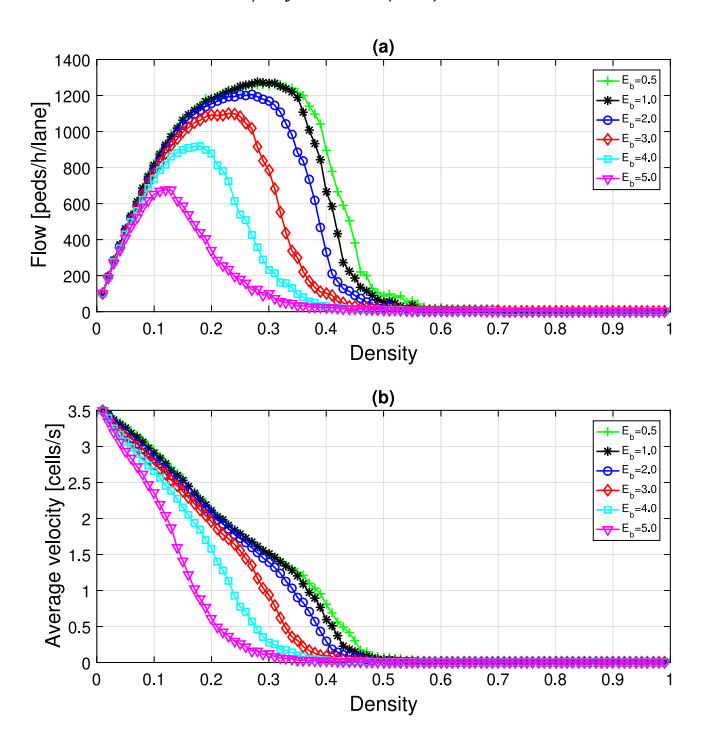


Fig. 4. Comparison results of the bi-direction pedestrian flow model with six different values of the interaction strength E_b from 0.5 to 5.0. In all KMC simulations, we take the lattice size M = 50, the directional split $N_W/N_E = 50/50$, the interaction strengths $E_a = 0$, $E_c = 10.0$, $E_d = E_b + 2.0$, $E_e = 12.0$, $E_f = E_b + 4.0$, $E_g = 14.0$, $E_h = 16.0$ and the final time is 2h. For every value of ρ and E_b , we report results averaged over ten simulations with different random number seeds. (a): Long-time averages of the density-flow relationship of pedestrians. (b): Ensemble-averaged velocity of pedestrians versus the density.

 $\langle F \rangle$ also tends to increase. The reasons are the following. First, since the interaction strengths $E_{\rm b}=2.0$, $E_{\rm c}=2.0+\delta E$, etc., the repulsion from both left and right side positions are relatively weak and the pedestrians can move sidewards from time to time, no matter whether they encounter other pedestrians with the opposite moving direction or with the different speed. Second, when the pedestrians encounter others with the opposite moving direction or with the slower speed, they need to move sidewards. But for the cases $\delta E=0$ or small value 1.0, they have no or very weak walking preference, so they may choose either side. Thus the pedestrians with opposite moving directions or with different speeds may have very frequent interactions, which produces completely jammed cases more often as shown in Fig. 2(c). Therefore, the transitions to jammed phases happen at lower densities for these smaller strengths of δE . On the other hand, when δE gets larger, the encountering pedestrians have stronger preference for the right-hand side to pass each other, and the fast pedestrians have stronger preference for the left-hand side to exceed the slow ones. So the system is self-organized into a partially jammed phase or a lane formation phase as shown in Figs. 2(d)(e)(f), where each type of pedestrians can move in their own zones or lanes. In this way, it allows a certain amount of flow and velocity. Hence, for the larger strengths of δE , the transitions to jammed phases happen at relatively larger densities.

Fig. 4 shows another set of comparison results of the density-flow and density-velocity curves, which use six different values of the interaction strength E_b from 0.5 to 5.0 with the fixed relationships $E_d = E_b + 2.0$ and $E_f = E_b + 4.0$. For the other interaction strengths, we take $E_a = 0$, $E_c = 10.0$, $E_e = 12.0$, $E_g = 14.0$, and $E_h = 16.0$, which corresponds to the case $\delta E = 8.0$ in the previous comparison result shown in Fig. 3. Therefore, the blue circles in Figs. 3 ($\delta E = 8.0$) and 4 ($E_b = 2.0$) represent the same results.

In Fig. 4, we observe that both the value of the critical density ρ_{crit} of the transition and the maximum value of the flow $\langle F \rangle$ decrease as the strength E_{b} increases. Moreover, during the transition, both the values of the flow $\langle F \rangle$ and the ensemble-averaged velocity $\langle v \rangle$ decrease with increasing strength E_{b} from 0.5 to 5.0 at the same total density ρ . The reasons also include two parts. First, since the interaction strength $E_{\text{c}} = 10.0$, etc., the repulsion from both left and right side positions are already extremely strong, pedestrians prefer to move straightforward towards their destinations. Only when they encounter other pedestrians with the opposite moving direction or with the different speed, they may move into their side positions. Second, if the situations shown in Figs. 1(d)(e) happen, the walking preference for the side positions in red also becomes weak as the strength E_{b} increases from 0.5 to 5.0. Thus the two species of pedestrians prefer to move straightforward towards their destinations in opposite directions, which produces completely jammed cases more often. Therefore, the transitions to jammed phases happen at lower densities for the larger strengths of E_{b} . On the other hand, when E_{b} is smaller (≤ 3.0), the pedestrians have stronger walking preference for the side positions and

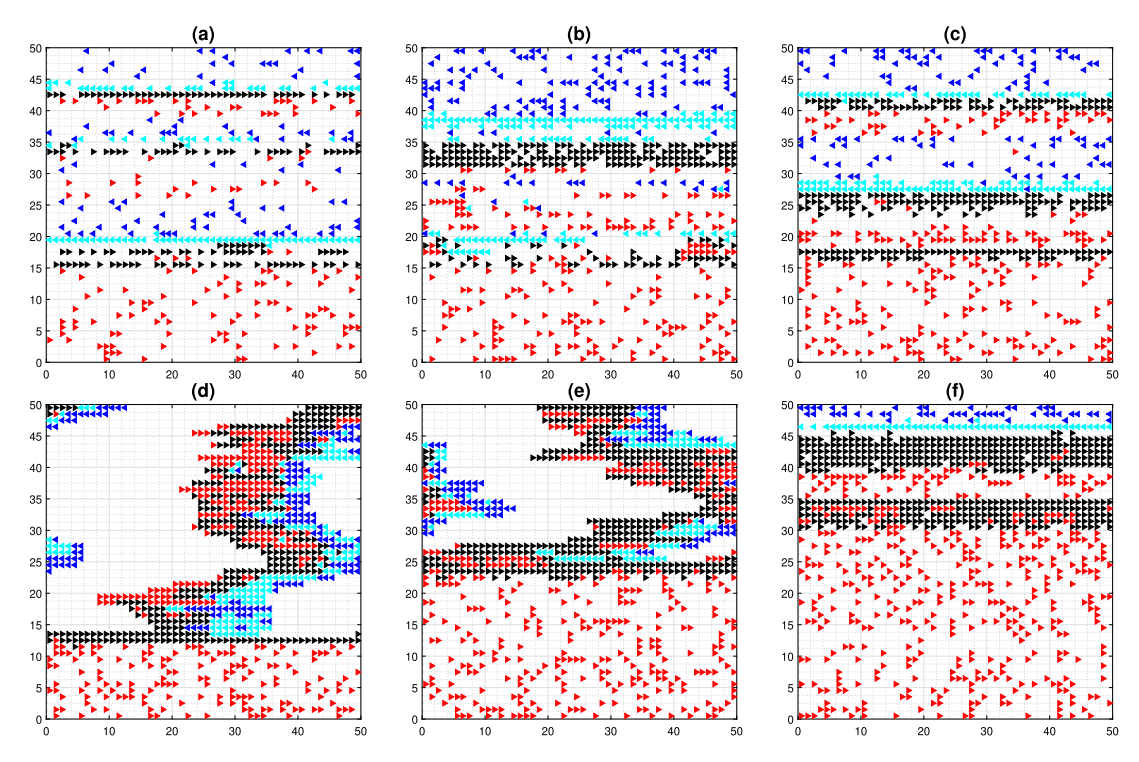


Fig. 5. Typical configurations of the bi-direction fast and slow pedestrian flow on an $M \times M$ lattice of size M = 50. The pedestrians are represented by red (►) for the slow eastbound, black (►) for the fast eastbound, blue (◄) for the slow westbound, and cyan (◄) for the fast westbound, respectively. In all KMC simulations, we take the interaction strengths $E_a = 0$, $E_b = 2.0$, $E_c = 10.0$, $E_d = 4.0$, $E_e = 12.0$, $E_f = 6.0$, $E_g = 14.0$, $E_h = 16.0$ and the final time is 2h. (a) A lane formation phase with the density $\rho = 0.2$ and the directional split $N_W/N_E = 40/60$. (b) A lane formation phase with $\rho = 0.3$ and $N_W/N_E = 30/70$. (d) A partially jammed phase with $\rho = 0.4$ and $N_W/N_E = 30/70$. (e) A partially jammed phase with $\rho = 0.4$ and $N_W/N_E = 30/70$. (e) A partially jammed phase with $\rho = 0.4$ and $N_W/N_E = 20/80$. (f) A lane formation phase with $\rho = 0.4$ and $N_W/N_E = 10/90$.

the system is self-organized into a partially jammed phase or a lane formation phase, which allows a certain amount of flow and velocity. Therefore, for the smaller strengths of $E_{\rm b}$, the transitions to jammed phases happen at relatively larger densities.

4.2. Numerical comparisons for different directional splits between pedestrians

Here, we perform a series of simulations with different values of directional splits $N_{\rm W}/N_{\rm E}$ between the westbound and eastbound pedestrians. For example, when the directional split $N_{\rm W}/N_{\rm E}=30/70$, the proportions of the two species of pedestrians in the total pedestrians are 30% and 70%, respectively. In this section, we take the strengths $E_{\rm a}=0$, $E_{\rm b}=2.0$, $E_{\rm c}=10.0$, $E_{\rm d}=4.0$, $E_{\rm e}=12.0$, $E_{\rm f}=6.0$, $E_{\rm g}=14.0$, and $E_{\rm h}=16.0$, which correspond to the case $\delta E=8.0$ in Fig. 3.

Fig. 5 shows six typical configurations of the bi-direction pedestrian flow with different values of the total density ρ and the directional splits $N_{\rm W}/N_{\rm E}$. Fig. 5(a) displays a lane formation phase with a low pedestrian density $\rho=0.2$ and the directional split $N_{\rm W}/N_{\rm E}=40/60$, where the pedestrians are separated into different lanes. Fig. 5(b) shows again a lane formation phase with an increased density $\rho=0.3$ and the same directional split $N_{\rm W}/N_{\rm E}=40/60$. After we change the directional split to $N_{\rm W}/N_{\rm E}=30/70$ with the same density $\rho=0.3$ in Fig. 5(c), the system is self-organized into another lane formation phase. However, when we increase the total density to $\rho=0.4$ with the same directional split $N_{\rm W}/N_{\rm E}=30/70$ in Fig. 5(d), a partially jammed phase appears where a big jam has formed in the upper and middle regions and blocks about 2/3 of the walkway, while part of the eastbound pedestrians are moving in the lower region. Fig. 5(e) shows again a partially jammed phase with the same density $\rho=0.4$ and a decreased directional split 20/80, where a smaller jam has formed and blocks about half of the walkway, and the lower region is dominated by the eastbound pedestrians. Once we change the directional split to $N_{\rm W}/N_{\rm E}=10/90$ with the same density $\rho=0.4$ in Fig. 5(f), the system is self-organized back into a lane formation phase. Here the westbound pedestrians walk in the region that is about 10% of the lattice and the eastbound pedestrians' region occupies the rest of the lattice.

For comparison, Fig. 6 shows the fundamental diagrams of the density-flow and density-velocity relationships with six different directional splits, specified in 10% increments from $N_W/N_E = 0/100$ (unidirectional flow) to $N_W/N_E = 50/50$ (balanced flow). We note that the blue circles in Fig. 6 ($N_W/N_E = 50/50$) and Fig. 3 ($\delta E = 8.0$) represent the same results. Here, all curves exhibit phase transitions between the free-flow phase and the jammed phase as the total

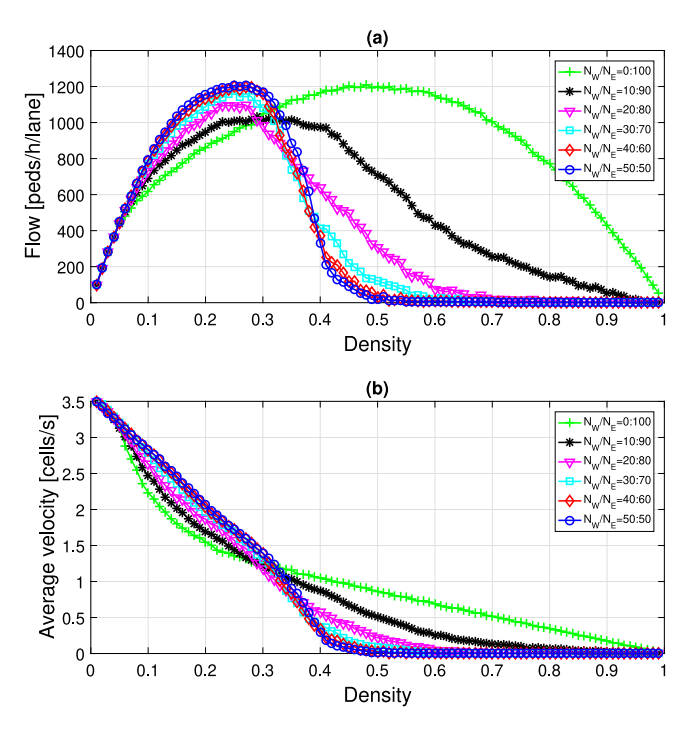


Fig. 6. Comparison results of the bi-direction pedestrian flow model with six different values of the directional splits N_W/N_E from 0/100 to 50/50. In all KMC simulations, we take the lattice size M=50, the interaction strengths $E_a=0$, $E_b=2.0$, $E_c=10.0$, $E_d=4.0$, $E_e=12.0$, $E_f=6.0$, $E_g=14.0$, $E_h=16.0$ and the final time is 2 h. For every value of ρ and N_W/N_E , we report results averaged over ten simulations with different random number seeds. (a): Long-time averages of the density-flow relationship of pedestrians. (b): Ensemble-averaged velocity of pedestrians versus the density.

density ρ increases. We also observe that for non-unidirectional flows, the density-flow and density-velocity curves of $N_{\rm W}/N_{\rm E}=40/60$ and 50/50 approximately resemble each other and are overlapped to some extent.

In Fig. 6, we observe that as the directional split changes from 0/100 to 20/80, the value of the critical density $\rho_{\rm crit}$ of the transition tends to decrease. For the cases of $N_{\rm W}/N_{\rm E}=20/80$ to 50/50, the critical density $\rho_{\rm crit}$ is about the same. Meanwhile, the maximum value of the flow $\langle F \rangle$ increases as $N_{\rm W}/N_{\rm E}$ changes from 10/90 to 50/50. When $\rho > 0.4$, both the values of the flow $\langle F \rangle$ and the ensemble-averaged velocity $\langle v \rangle$ decrease with increasing directional split from 0/100 to 50/50 at the same total density ρ . This is because in the bi-direction model, the two species of pedestrians move in only two opposite directions, so the interference is mainly from the encountering flows. When the direction split is small, say $N_{\rm W}/N_{\rm E}=10/90$, there is a big difference in the numbers of two species of pedestrians. The movement of the pedestrians dominant in number (eastbound) has more effect than the movement of their opponents (westbound). The jammed area is limited and can only block a small portion of the dominant pedestrians (eastbound), which produces relatively higher values of $\langle F \rangle$ and $\langle v \rangle$. When the direction split increases, the disparity between the numbers of two species of pedestrians becomes smaller. Therefore, the two effects of the encountering flows become equally strong, which produces larger jammed areas. Hence, the values of $\langle F \rangle$ and $\langle v \rangle$ decrease in this regard. This observation has been shown in Figs. 5(d)–(f) where the direction split changes from 30/70 to 10/90.

4.3. Numerical comparisons with empirical data

Finally, we compare the simulation results of the fundamental density–flow and density–velocity relationships with the empirical data shown in [74,75] for various types of infrastructure, flow composition, etc. derived from Fruin [76], Weidmann [77], Virkler and Elayadath [78], Older [79], Sarkar and Janardhan [80] and Tanariboon et al. [81]. For comparison in Fig. 7, we adopt the units used in [74]: flow in peds/s/m, velocity in m/s, and density in peds/m². As we set the physical size of each cell to $0.4 \times 0.4 = 0.16$ m², there are about six pedestrians per square meter (peds/m²). Therefore, when the density reaches $\rho = 1.0$ in our simulations, all the cells on the lattice are occupied by pedestrians, which is equivalent to 6 peds/m² in real situations [10,71]. Again, we set the fast pedestrians' desired speed to 4 cells/s and the slow ones' to 3 cells/s, which corresponds to ≈ 1.6 m/s (business) and ≈ 1.2 m/s (leisure), respectively [10].

In Fig. 7, we use two simulation results with the strengths $E_a = 0$, $E_b = 2.0$, $E_c = 10.0$, $E_d = 4.0$, $E_e = 12.0$, $E_f = 6.0$, $E_g = 14.0$, and $E_h = 16.0$, which correspond to the case $\delta E = 8.0$ in Fig. 3. Both of simulation cases are with the system size M = 10: one case for the directional split $N_W/N_E = 10/90$ (labeled by the black stars) and the other case for $N_W/N_E = 50/50$ (labeled by the blue circles). We can see that both the average flow $\langle F \rangle$ and the ensemble-averaged

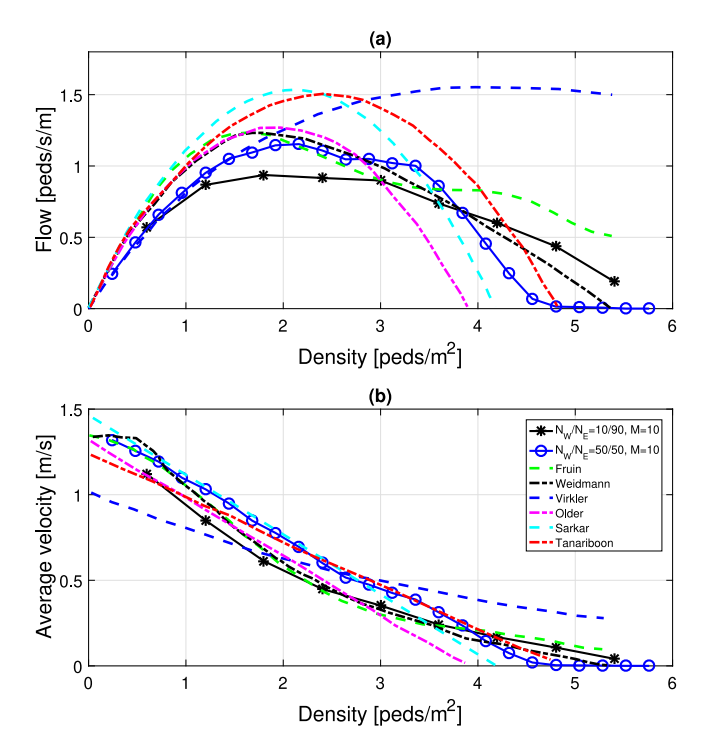


Fig. 7. Comparison results of the bi-direction pedestrian flow model with empirical data from [74,75]. Both of simulation cases are with the interaction strengths $E_a = 0$, $E_b = 2.0$, $E_c = 10.0$, $E_d = 4.0$, $E_e = 12.0$, $E_f = 6.0$, $E_g = 14.0$, $E_h = 16.0$, the system size M = 10 and the final time is 2h. One simulation case is for the directional split $N_W/N_E = 10/90$. The other one is for $N_W/N_E = 50/50$. (a): The density-relationship of pedestrians. (b): The density-velocity relationship of pedestrians.

velocity $\langle v \rangle$ in the two simulation results have good match with some empirical data as the density ρ increases, except that the average flow $\langle F \rangle$ of the case $N_{\rm W}/N_{\rm E}=10/90$ is slightly below the empirical data around $\rho_{\rm crit}$ when the flow reaches its maximum. The reason of deviation may be due to the simplification of the discrete cellular automaton model, which allows the pedestrians move in only eight directions and cannot fully represent the continuity of pedestrians' movement and limit their freedom. Meanwhile, the current model treats the pedestrians as individual agents with the same characteristics and ignores the diversity of pedestrians in reality, such as differences in purpose, age, gender, etc. [10]. Moreover, we propose our lattice model in a closed system and take the periodic and closed boundary conditions without external interference, while in real situations pedestrian flows may be affected by many external factors. Therefore, there are some deviations between our simulation results and the empirical data.

5. Conclusions

In this paper, the kinetic Monte Carlo (KMC) method for a 2D cellular automaton (CA) model has been used to study the bi-direction pedestrian flows with different walk speeds. The models considered here incorporate the traffic rules and customs through the transition rates in different moving directions and the interactions between pedestrians. To simulate the time evolution of the pedestrian system, we developed an efficient list-based KMC algorithm using fast search that can further improve computational efficiency. In the KMC method, the dynamics of pedestrians is described in terms of the transition rates corresponding to possible configurational changes of the system, and then the corresponding time evolution of the system can be expressed in terms of these rates. The KMC simulations relied on the calibration of model parameters: the characteristic time τ_{fast} and τ_{slow} and the strength parameters of pedestrian interactions, E_{a} to E_{h} . Then we use the KMC simulations to quantitatively predict the time evolution of the bi-direction pedestrian flows with different walk speeds.

The simulations focus on two aspects: different strengths of walking preference and different directional splits of the pedestrians. For both aspects, we obtained fundamental diagrams which display several observed traffic states. Both results exhibit a phase transition from freely flowing to fully jammed, as a function of initial total density of pedestrians. Through comparison between the KMC simulation results and the empirical data, we find that the pedestrian model can show some typical self-organization phenomena in certain parameter regimes and reflect transition trends of the corresponding empirical data from real traffic. In particular, this model can reproduce the phenomenon observed empirically, lane formation, where the fast pedestrians exceed the lower ones through a narrow walkway.

Declaration of competing interest

The authors declare that they have no known competing financial interests or personal relationships that could have appeared to influence the work reported in this paper.

CRediT authorship contribution statement

Yi Sun: Conceptualization, Data curation, Formal analysis, Funding acquisition, Investigation, Methodology, Project administration, Resources, Software, Supervision, Validation, Visualization, Writing - original draft, Writing - review & editing.

Acknowledgments

The research is partially supported by the U.S. National Science Foundation under grant numbers DMS-1620212, DMS-1913146 and a SC EPSCoR GEAR-CRP, USA Award.

References

- [1] K. Nagel, J. Esser, M. Rickert, Large-scale traffic simulations for transportation planning, in: D. Stauffer (Ed.), Annual Reviews of Computational Physics, World Scientific, Singapore, 2000, pp. 151–202.
- [2] D. Chowdhury, L. Santen, A. Schadschneider, Statistical physics of vehicular traffic and some related systems, Phys. Rep. 329 (2000) 199-329.
- [3] D. Helbing, Traffic and related self-driven many-particle systems, Rev. Modern Phys. 73 (2001) 1067-1141.
- [4] T. Nagatani, The physics of traffic jams, Rep. Progr. Phys. 65 (2002) 1331-1386.
- [5] B.S. Kerner, The Physics of Traffic, Springer, Heidelberg, 2004.
- [6] S. Maerivoet, B. De Moor, Cellular automata models of road traffic, Phys. Rep. 419 (2005) 1-64.
- [7] B.S. Kerner, Introduction to Modern Traffic Flow Theory and Control: The Long Road to Three-Phase Traffic Theory, Springer, Heidelberg, 2009.
- [8] R. Kühne, N.H. Gartner (Eds.), 75 Years of the Fundamental Diagram for Traffic Flow Theory: Greenshields Symposium, Transportation Research Board, Washington, DC, 2011.
- [9] N. Bellomo, C. Dogbe, On the modeling of traffic and crowds: A survey of models, speculations, and perspectives, SIAM Rev. 53 (2011) 409-463.
- [10] A. Schadschneider, D. Chowdhury, K. Nishinari, Stochastic Transport in Complex Systems, Elsevier, The Netherlands, 2011.
- [11] M. Treiber, A. Kesting, Traffic Flow Dynamics: Data, Models and Simulation, Springer, Heidelberg, 2013.
- [12] D. Ni, Traffic Flow Theory Characteristics, Experimental Methods, and Numerical Techniques, Elsevier, The Netherlands, 2016.
- [13] M. Schreckenberg, S.D. Sharma (Eds.), Pedestrian and Evacuation Dynamics, Springer, Berlin, 2002.
- [14] A. Schadschneider, Traffic flow: a statistical physics point of view, Physica A 313 (2002) 153–187.
- [15] E.R. Galea (Ed.), Pedestrian and Evacuation Dynamics, CMS Press, London, 2003.
- [16] U. Weidmann, U. Kirsch, M. Schreckenberg (Eds.), Pedestrian and Evacuation Dynamics, Springer, Berlin, 2014.
- [17] E. Cristiani, B. Piccoli, A. Tosin, Multiscale Modeling of Pedestrian Dynamics, Springer, Berlin, 2014.
- [18] L.F. Henderson, On the fluid mechanics of human crowd motion, Transp. Res. 8 (1974) 509–515.
- [19] D. Helbing, A fluid dynamic model for the movement of pedestrians, Complex Systems 6 (1992) 391-415.
- [20] R.L. Hughes, A continuum theory for the flow of pedestrians, Transp. Res. B 36 (2002) 507-535.
- [21] R.L. Hughes, The flow of human crowds, Annu. Rev. Fluid Mech. 35 (2003) 169-182.
- [22] N. Bellomo, C. Dogbe, On the modelling crowd dynamics: From scaling to second order hyperbolic macroscopic models, Math. Models Methods Appl. Sci. 18 (2008) 1317–1345.
- [23] L. Huang, S.C. Wong, M. Zhang, C.-W. Shu, W.H.K. Lam, Revisiting Hughes' dynamic continuum model for pedestrian flow and the development of an efficient solution algorithm, Transp. Res. B 43 (2009) 127–141.
- [24] A. Chertock, A. Kurganov, A. Polizzi, I. Timofeyev, Pedestrian flow models with slowdown interaction, Math. Models Methods Appl. Sci. 24 (2014) 249–275.
- [25] D. Helbing, P. Molnár, Social force model for pedestrian dynamics, Phys. Rev. E 51 (1995) 4282.
- [26] D. Helbing, I. Farkas, T. Vicsek, Simulating dynamical features of escape panic, Nature 407 (2000) 487-490.
- [27] D. Helbing, I. Farkas, T. Vicsek, Freezing by heating in a driven mesoscopic system, Phys. Rev. Lett. 84 (2000) 1240-1243.
- [28] A. Nakayama, K. Hasebe, Y. Sugiyama, Instability of pedestrian flow and phase structure in a two-dimensional optimal velocity model, Phys. Rev. E 71 (2005) 036121.
- [29] A. Nakayama, K. Hasebe, Y. Sugiyama, Effect of attractive interaction on instability of pedestrian flow in a two-dimensional optimal velocity model, Phys. Rev. E 77 (2008) 016105.
- [30] S. Wolfram, Theory and Applications of Cellular Automata, World Scientific, Singapore, 1986.
- [31] S. Wolfram, Cellular Automata and Complexity, Addison-Wesley, Reading, MA, 1994.
- [32] M. Cremer, J. Ludwig, A fast simulation model for traffic flow on the basis of boolean operations, Math. Comput. Simulation 28 (1986) 297-303.
- [33] K. Nagel, M. Schreckenberg, A cellular automaton model for freeway traffic, J. Physique I 2 (1992) 2221-2229.
- [34] O. Biham, A.A. Middleton, D. Levine, Self-organization and dynamical transition in traffic-flow models, Phys. Rev. A 46 (1992) R6124-6127.
- [35] R. Barlovic, L. Santen, A. Schadschneider, M. Schreckenberg, Metastable states in cellular automata for traffic flow eur, J. Phys. B 5 (1998) 793–800
- [36] W. Knospe, L. Santen, A. Schadschneider, M. Schreckenberg, Towards a realistic microscopic description of highway traffic, J. Phys. A 33 (2000) 1477.
- [37] W. Knospe, L. Santen, A. Schadschneider, M. Schreckenberg, Single-vehicle data of highway traffic: Microscopic description of traffic phases, Phys. Rev. E 65 (2002) 056133.
- [38] P. Nelson, On driver anticipation, two-regime flow, fundamental diagrams, and kinematic-wave theory, Transp. Sci. 40 (2006) 165-178.
- [39] A. Sopasakis, M.A. Katsoulakis, Stochastic modeling and simulation of traffic flow: Asymmetric single exclusion process with arrhenius look-ahead dynamics, SIAM J. Appl. Math. 66 (2006) 921–944.
- [40] N. Dundon, A. Sopasakis, Stochastic modeling and simulation of multi-lane traffic, Transp. Traffic Theory 17 (2007) 661-691.
- [41] T. Alperovich, A. Sopasakis, Stochastic description of traffic flow, J. Stat. Phys. 133 (2008) 1083–1105.
- [42] C. Hauck, Y. Sun, I. Timofeyev, On cellular automata models of traffic flow with look ahead potential, Stoch. Dynam. 14 (2014) 1350022.

- [43] Y. Sun, I. Timofeyev, Kinetic Monte Carlo simulations of one-dimensional and two-dimensional traffic flows: Comparison of two look-ahead rules, Phys. Rev. E 89 (2014) 052810.
- [44] Y. Sun, C. Tan, On a class of new nonlocal traffic flow models with look-ahead rules, 2020, arXiv:2001.10017.
- [45] V.J. Blue, J.L. Adler, Emergent fundamental pedestrian flows from cellular automata microsimulation, Transp. Res. Rec. 1644 (1998) 29-36.
- [46] V.J. Blue, J.L. Adler, Cellular automata microsimulation of bidirectional pedestrian flows, Transp. Res. Rec. 1678 (1999) 135–141.
- [47] V.J. Blue, J.L. Adler, Modeling four-directional pedestrian flows, Transp. Res. Rec. 1710 (2000) 20-27.
- [48] V.J. Blue, J.L. Adler, Cellular automata microsimulation for modeling bi-directional pedestrian walkways, Transp. Res. B 35 (2001) 293-312.
- [49] M. Fukui, Y. Ishibashi, Self-organized phase transitions in cellular automaton models for pedestrians, J. Phys. Soc. Japan 68 (1999) 2861.
- [50] M. Fukui, Y. Ishibashi, Jamming transition in cellular automaton models for pedestrians on passageway, J. Phys. Soc. Japan 68 (1999) 3738.
- [51] M. Muramatsu, T. Irie, T. Nagatani, Jamming transition in pedestrian counter flow, Physica A 267 (1999) 487-498.
- [52] M. Muramatsu, T. Nagatani, Jamming transition in two-dimensional pedestrian traffic, Physica A 275 (2000) 281-291.
- [53] M. Muramatsu, T. Nagatani, Jamming transition of pedestrian traffic at a crossing with open boundaries, Physica A 286 (2000) 377–390.
- [54] K. Takimoto, T. Nagatani, Spatio-temporal distribution of escape time in evacuation process, Physica A 320 (2003) 611-621.
- [55] C. Burstedde, K. Klauck, A. Schadschneider, J. Zittarz, Simulation of pedestrian dynamics using a two-dimensional cellularautomaton, Physica A 295 (2001) 507–525.
- [56] A. Kirchner, A. Schadschneider, Simulation ofevacuation processes using a bionics-inspired cellular automaton model for pedestrian dynamics, Physica A 312 (2002) 260–276.
- [57] H. Yue, H. Hao, X. Chen, C. Shao, Simulation of pedestrian flow on square lattice based on cellular automata model, Physica A 384 (2007) 567–588.
- [58] H. Yue, H. Guan, J. Zhang, C. Shao, Study on bi-direction pedestrian flow using cellular automata simulation, Physica A 389 (2010) 527-539.
- [59] W.F. Fang, L.Z. Yang, W.C. Fan, Simulation of bi-direction pedestrian movement using a cellular automata model, Physica A 321 (2003) 633-640.
- [60] J. Li, L. Yang, D. Zhao, Simulation of bi-direction pedestrian movement in corridor, Physica A 354 (2005) 619-628.
- [61] W.G. Weng, T. Chen, H.Y. Yuan, W.C. Fan, Cellular automaton simulation of pedestrian counter flow with different walk velocities, Phys. Rev. E 74 (2006) 036102.
- [62] L. Yang, J. Li, S. Liu, Simulation of pedestrian counter-flow with right-moving preference, Physica A 387 (2008) 3281-3289.
- [63] Y. Sun, Kinetic Monte Carlo simulations of two-dimensional pedestrian flow models, Physica A 505 (2018) 836-847.
- [64] Y. Sun, Simulations of bi-direction pedestrian flow using kinetic Monte Carlo methods, Physica A 524 (2019) 519-531.
- [65] A.B. Bortz, M.H. Kalos, J.L. Lebowitz, A new algorithm for Monte Carlo simulation of ising spin systems, J. Comput. Phys. 17 (1975) 10-18.
- [66] T.D. Liggett, Interacting Particle Systems, Springer, Berlin, 1985.
- [67] N. Metropolis, A.E. Rosenbluth, M.N. Rosenbluth, A.H. Teller, E. Teller, Equation of state calculations by fast computing machines, J. Chem. Phys. 21 (1953) 1087.
- [68] J.L. Blue, I. Beichl, F. Sullivan, Faster Monte Carlo simulations, Phys. Rev. E 51 (1995) R867.
- [69] T.P. Schulze, Kinetic Monte Carlo simulations with minimal searching, Phys. Rev. E 65 (2002) 036704.
- [70] Y. Sun, R. Caflisch, B. Engouist, A multiscale method for epitaxial growth, SIAM Multiscale Model, Simul, 9 (2011) 335–354.
- [71] S. Buchmueller, U. Weidmann, Parameters of Pedestrians Pedestrian Traffic and Walking Facilities, in: Schriftenreihe des IVT, vol. 132, ETH Zürich. 2007.
- [72] B.D. Greenshields, A study of traffic capacity, Proc. Highw. Res. Board 14 (1935) 448-477.
- [73] R.T. Underwood, Speed, Volume, and Density Relationships: Quality and Theory of Traffic Flow, 141, Yale Bureau of Highway Traffic, 1961.
- [74] W. Daamen, S.P. Hoogendoorn, P.H.L. Bovy, First-order pedestrian traffic flow theory, in: Transportation Research Board 84th Annual Meeting, National Academy Press, Washington DC, 2005.
- [75] L.D. Vanumu, K.R. Rao, G. Tiwari, Fundamental diagrams of pedestrian flow characteristics: A review, Eur. Transp. Res. Rev. 9 (2017) 49.
- [76] J.J. Fruin, Design for pedestrians: A level-of-service concept, High. Res. Record 355 (1971) 1-15.
- [77] U. Weidmann, Transporttechnik der FußGäNger, Schriftenreihe des IVT, vol. 80, ETH Zürich, 1993 (in German, for english translation see [71]).
- [78] M.R. Virkler, S. Elayadath, Pedestrian speed-flow-density relationships, Transp. Res. Rec. 1438 (1994) 51-58.
- [79] S.J. Older, Movement of pedestrians on footways in shopping streets, Traffic Engineering and Control 10 (1968) 160-163.
- [80] A.K. Sarkar, K.S.V.S. Janardhan, A study on pedestrian flow characteristics, in: Proceedings, Transportation Research Board, Washington, DC, 1997.
- [81] Y. Tanariboon, S.S. Hwa, C.H. Chor, Pedestrian characteristics study in Singapore, ASCE J. Transp. Eng. 112 (1986) 229-235.